JOURNAL OF CATALYSIS 157, 51–65 (1995)

Infrared Study of the Dynamics of Adsorbed Species during CO Hydrogenation

Michael W. Balakos,[1] Steven S. C. Chuang,[2] Girish Srinivas,[3] and Mark A. Brundage

The University of Akron, Department of Chemical Engineering, Akron, Ohio 44325-3906

Received December 5, 1994; revised May 25, 1995; accepted July 26, 1995

The dynamics of adsorbed species on Rh/SiO_2 catalyst during CO hydrogenation to form methane was studied using *in situ* infrared (IR) spectroscopy combined with steady-state isotopic transient and pulsing CO methods. *In situ* IR spectra and transient responses reveal that gaseous CO rapidly exchanges with adsorbed CO and hydrogenation of CH_x intermediate is the rate-determining step under steady-state conditions. Compartment modeling and site distribution analysis of the transient responses show that CH_x is hydrogenated to CH_4 with a bimodal distribution of the rate constant. When CO is pulsed into H_2 flow, CO dissociation is the rate-determining step and linear CO depletes faster than bridged CO. The rate-determining step for methanation is a delicate balance of intermediate concentrations, surface intrinsic properties, and reaction conditions. Mechanistic and kinetic studies of catalytic reactions have to be performed under practical reactor conditions. © 1995 Academic Press, Inc.

INTRODUCTION

Dynamic (transient-response) methods have been widely used in scientific research in order to gain an understanding of the dynamics of various processes. The dynamic method involves a sudden change (stimulus) to an input of a system and recording the output (response). This method has been used in fields such as biology (1), physiology (2), pharmacokinetics (3), and chemical kinetics (4). The transient-response technique has also long been used by chemical engineers for many decades (5–8). This technique has been used to study the flow characteristics and dynamics of process equipment such as heat exchangers, distillation columns, and chemical reactors. During the past 20 years, advances in analytical instrumentation have made possible the use of transient techniques in the field of catalysis. For the dynamic measurement of heterogeneous catalytic reactions, the forcing function (stimulus or input function) is a change in the conditions of the reaction. The response of the reaction products is monitored as a function of time. The resulting response contains valuable information on the kinetics and mechanism of the surface reactions (9).

Many forcing functions may be applied to a reaction system for the elucidation of the dynamics of elementary reactions and the kinetics of overall reactions. A stimulus to the input concentrations of the reactants is the most common dynamic approach in heterogeneous catalysis. The type of applied forcing function to the feed to the reactor includes a step change (10), a pulse (11), a ramp function (12), and an oscillating function (13). Four types of input functions have been used to study CO hydrogenation over various types of catalysts. These input functions include (i) a step change in the inlet CO concentration, (ii) a pulse of CO into an inlet H_2 flow, (iii) a pulse of isotopic ^{13}CO into the inlet CO flow, and (iv) a step change in the inlet CO concentration replaced by isotopic ^{13}CO. In the latter two cases, the overall flow of CO and ^{13}CO is maintained at steady-state. Due to the complexity of the kinetics and mechanism of CO hydrogenation, the information gained from such experiments depends on the type of experiment performed.

Methanation, the reaction of CO/H_2 to form methane, on Group VIII metals is the subject of many investigations (14–22). Despite the amount of literature, a controversy exists concerning the mechanism centering on the rate-determining step for the formation of methane on Group VIII metal catalysts (23). Using pulse surface reaction rate analysis and/or temperature-programmed reaction studies, it has been concluded that CO dissociation is the rate-determining step on supported Ni and Rh (11, 24–28). On the other hand, by measuring the initial behavior of the methanation reaction on Ni, Araki and Ponec (29) elucidated that the hydrogenation of surface CH_x intermediates is the rate-determining step. This proposition was later supported by transient and steady-state isotopic transient experiments on supported Ni, Co, and Ru (30–34). An Auger Electron Spectroscopy study of a Ni(100) surface

[1] Present address: United Catalysts Inc., Louisville, Kentucky.
[2] To whom correspondence should be addressed.
[3] Present address: TDA Research, Inc., Wheat Ridge, Colorado.

0021-9517/95 $12.00

revealed that the rate of CO dissociation and the rate of CH_x hydrogenation are comparable and that "neither of these is rate-determining in the usual sense" (35, 36). Bennett and co-workers (37, 38) have also concluded from transient studies that no clear rate-determining step exists for the methanation reaction on supported Ni and Rh catalysts. It is well known that different catalysts for the same reaction may have different rate-determining steps (16). Different conditions for mechanistic studies may lead to different conclusions about the mechanism and which elementary step is rate-determining for the methanation reaction.

The objective of this paper is to investigate the kinetics and mechanism of methanation on Rh/SiO_2 catalyst using transient response techniques. A combined *in situ* Fourier transform infrared spectroscopy (IR) and mass spectrometry (MS) reaction system was used in this study. The IR was used to monitor the transient response of the adsorbed species and the MS was used to monitor the response of the gaseous products. Two transient techniques used in this study include pulsing CO in a steady-state H_2/He flow and a switch between CO and ^{13}CO during steady-state CO hydrogenation on 3 wt% Rh/SiO_2 catalyst. Comparison of information gained from these techniques reveals the advantages and limitations of each for the mechanistic study. The kinetics and mechanism of CO hydrogenation on Rh/SiO_2 determined from these techniques will be compared with the literature to explain consistencies and discrepancies of the voluminous data on the methanation reaction on Group VIII metals in general, and on Rh in particular.

EXPERIMENTAL METHODS

Catalyst Preparation

A 3 wt% Rh/SiO_2 catalyst sample was prepared by incipient wetness. An aqueous solution of $Rh(NO_3)_3 \cdot 2H_2O$ (Johnson-Matthey Chemicals) was impregnated into a SiO_2 support (Strem Chemicals, No. 14-7420; SA, 350 m^2/g). After impregnation, the sample was dried overnight in air at 301 K and then reduced in flowing hydrogen at 673 K for 16 h. The final catalyst form was a fine black powder. The hydrogen uptake of the catalyst was measured at 303 K by the pulse adsorption method and was found to be 14.0 μmol/g. This corresponds to a dispersion of 0.096 and a crystallite size of 96 Å, assuming an adsorption stoichiometry of $H_{ads}/Rh = 1$ and a cubic shape of Rh crystallites (39).

Experimental Reactor System

The transient IR system used in this study is similar to the system reported in a previous study (40, 41). This system consists of a gas supply section, a reactor section, and an analysis section. The gas supply section contains the gases CO, H_2, He (Linde, Ultra High Purity Grade), and isotopic ^{13}CO (MSD Isotopes, 98% ^{13}C). The CO and H_2 were further purified by passing them over a molecular sieve. The He was passed over a molecular sieve and an oxygen trap. The ^{13}CO was not further purified. All gas flows were controlled by Brooks mass flow controllers (Model 5850E). The gas flow section also contains two pulsing valves and one switching valve. The first pulsing valve can pulse hydrogen or CO into the He stream. The second pulsing valve can pulse the isotopic ^{13}CO into the CO stream. The switching valve performs the step change between CO and isotopic ^{13}CO. The pulsing and switching valves are all zero dead volume Valco valves.

The reactor section contains a high temperature and pressure IR reactor cell consisting of four stainless steel flanges and two CaF_2 step windows (42). The catalyst powder was pressed into a disk and held between the two windows. The step windows minimize the reactor volume and reduce the optical path length for the gas phase in the reactor. The IR cell can be operated at temperatures up to 533 K and pressures up to 6.0 MPa. The reactor is heated by a heating tape wrap and the temperature is controlled by an Omega temperature controller (Model 2011k).

The analysis section consists of a Fourier transform infrared spectrometer (FTIR), a mass spectrometer (MS), and a gas chromatograph (GC). The infrared spectra of adsorbed species were recorded by a Nicolet 5SXC spectrometer with a DTGS detector at a resolution of 4 cm^{-1}. The transient responses of the gaseous products were analyzed by a Balzers QMG112 MS controlled by a microcomputer with a differentially pumped gas inlet system (Blazers GES 010). The inlet system allows a portion of the reactor effluent to be continuously sampled by a rotary vane pump through a capillary tube to a medium vacuum of approximately 0.7 mbar. A valve to the MS vacuum chamber ($\sim 5.0 \times 10^{-6}$ mbar) has an aperture that allows ~2% of the gas in the medium vacuum to enter the ionization chamber of the mass spectrometer. The two-stage configuration ensures that sampling is free from mass discrimination and has a fast response time. The capillary and vacuum chambers are kept at 473 K to prevent condensation of products. Steady-state product analysis is conducted online by a HP-5890A GC with an FID detector. The GC consists of a 1.8-m Poropak PS column in series with a 1.8-m Poropak QS column.

Transient Studies

The Rh/SiO_2 powder (63 mg) was pressed into a self-supporting disk and placed in the reactor. Prior to the transient study, the catalyst was reduced in flowing hydrogen at 503 K for 2 h. The isotopic switches between CO and isotopic ^{13}CO were all performed at 0.1 MPa. After

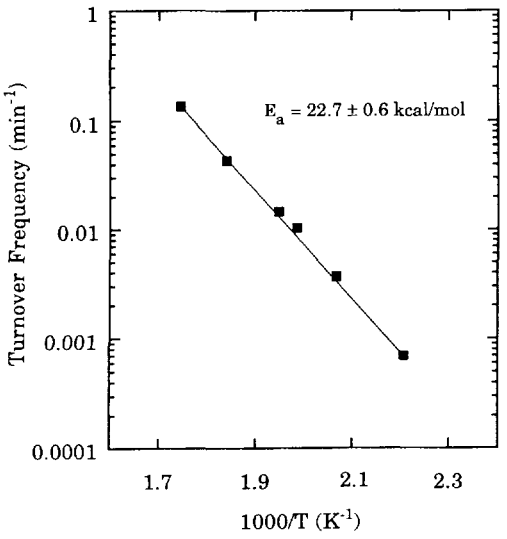

FIG. 1. Arrhenius plot of methanation on 3 wt% Rh/SiO_2 at 0.1 MPa and CO/H_2 = 1/1.

reduction at 503 K, the temperature was reduced to the reaction temperature under H_2 flow. A CO, H_2, and He mixture was passed over the catalyst at the flowrates of 10, 10, and 20 cm^3/min, respectively. The CO contains 2.01% Ar for determining the effect of gas holdup in the reactor and the gas transportation lines on the transient response of gaseous products. The average residence time of Ar determined from the transient response equals the sum of the residence times of reactant flow in the transportation lines, the reactor, and the MS inlet system. After 1 h of reaction time, the concentration of gaseous products was measured by gas chromatograph, and the reactant composition was switched from $CO/Ar/H_2/He$ (at a ratio of 1/0.02/1/2) to $^{13}CO/H_2/He$ (at a ratio of 1/1/2). Helium is an inert gas in the reaction and was used to keep the concentration of ionized species in the MS vacuum chamber low for high sensitivity to reaction products. The CO and ^{13}CO flowrates were kept the same to maintain the steady state of the reaction. The *m/e* ratios followed by the MS were 15 for CH_4, 28 for CO, 29 for ^{13}CO, and 40 for Ar. The *m/e* ratios were carefully selected to prevent interference from fragmentation of parent species.

Pulsing CO in H_2 flow was performed by pulsing 1 cm^3 of CO into an inert He flow of 25 cm^3/min and then mixed downstream with H_2 at a flow of 15 cm^3/min. This approach has been termed pulse surface reaction rate analysis by Mori *et al.* (11). The difference between Mori's approach and our method is that complete product analysis by MS was performed in our study while Mori's analysis involves monitoring only methane with a flame ionization detector. Adsorbed species and gaseous products were recorded by FTIR and MS, respectively. Transient response of methane was recorded at *m/e* of 15 in the MS to prevent interference from the secondary water peak at *m/e* of 16. Carbon dioxide and H_2O responses were also recorded at *m/e* of 44 and 18, respectively.

RESULTS

Steady-State Experiments

The methanation reaction was studied at steady state with CO/H_2 = 1/1 at 0.1 MPa and a temperature range of 453–573 K. The only hydrocarbon product observed was methane at temperatures below 503 K. At temperatures

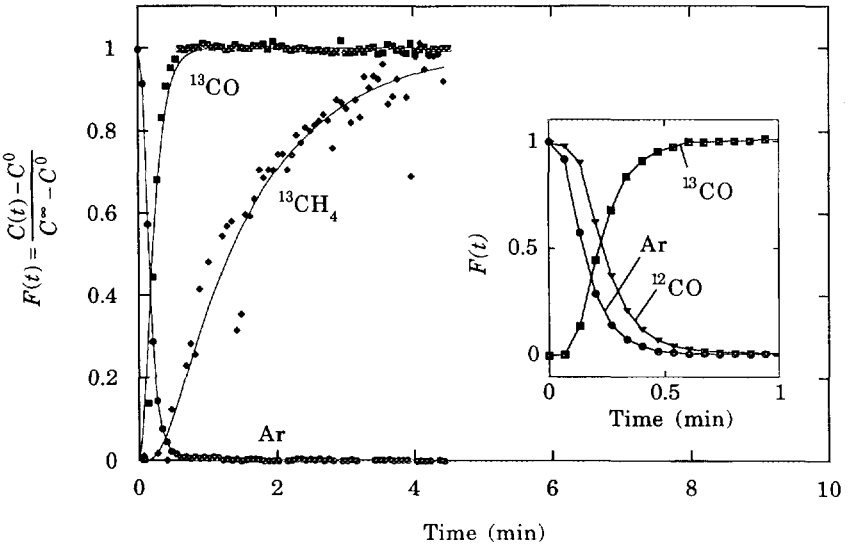

FIG. 2. Steady-state isotopic transient of methanation on 3 wt% Rh/SiO_2 at 453 K and 0.1 MPa.

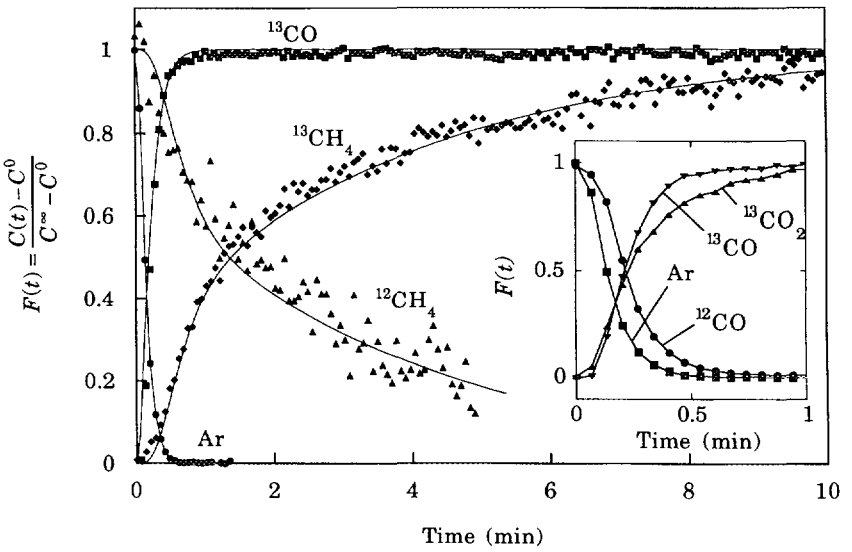

FIG. 3. Steady-state isotopic transient of methanation on 3 wt% Rh/SiO_2 at 503 K and 0.1 MPa.

above 503 K, trace amounts of ethylene and ethane were also observed. The turnover frequency (TOF) is defined as the number of moles of methane formed per minute per mole of surface-exposed Rh metal. Figure 1 is an Arrhenius plot of methanation from the steady-state experiments. A fit of the Arrhenius equation gives an activation energy of 22.7 ± 0.6 kcal/mol for methanation. This value agrees well with previous literature results on supported Rh catalysts (14, 43, 44).

Steady-State Isotopic Transient

The reactant feed was switched from $CO/Ar/H_2/He$ to $^{13}CO/H_2/He$ at three different temperatures, 453, 483, and 503 K. The IR recorded the vibrational spectra of the transients of adsorbed intermediates while the MS recorded the transient responses of CO, ^{13}CO, Ar, CH_4, and $^{13}CH_4$. For comparison, transient responses to a switch from CO to ^{13}CO were normalized using the equation

$$F_i(t) = \frac{y_i(t) - y_i^0}{y_i^\infty - y_i^0} = \frac{C_i(t) - C_i^0}{C_i^\infty - C_i^0}, \qquad [1]$$

where $F_i(t)$ is the fraction of the response of product i with respect to the change in concentration at time = 0 and time = ∞, $y_i(t)$ is the MS signal for a specific m/e ratio representing product i, and $C_i(t)$ is the concentration of product i.

The normalized Ar, ^{12}CO, ^{13}CO, and $^{13}CH_4$ responses to the switch from CO to ^{13}CO in the inlet flow are shown in Figs. 2 and 3 at 453 and 503 K, respectively. The response to a switch at 483 K was also recorded and reported (45). The Ar response is very rapid as compared to the CH_4 at both temperatures. The inset in each figure and the $^{12}CH_4$ response in Fig. 3 are shown to illustrate the symmetry in the response of the labeled and nonlabeled products. The symmetry in CO and ^{13}CO as well as CH_4 and $^{13}CH_4$ responses indicate that CO was replaced by ^{13}CO approximately at a one-to-one ratio during the switch from ^{12}CO to ^{13}CO. A symmetrical response indicates that the steady state was not disturbed during the course of the transient experiment. The CO response lags behind the Ar response by a small amount. The delay in the CO response with respect to Ar indicates adsorption and desorption of CO on the surface of the catalyst. The $^{13}CH_4$ response was slow compared to the ^{13}CO response, indicating a large average residence time for carbon-containing intermediates leading to the formation of methane. Comparison of $^{13}CH_4$ response at 453 and 503 K shows that the residence time of intermediates (i.e., time constant) for the methane response increased with an increase in temperature. Carbon dioxide was also produced during methanation at 483 and 503 K. The CO_2 response is significantly faster than that of CH_4 and did not vary significantly with temperature.

The IR spectra corresponding to the MS response to the isotopic switch at 453 K are shown in Fig. 4. The IR spectroscopy of the step switches at 483 and 503 K yield similar results. Due to the use of step windows for minimizing the IR beam path through the gas phase of the reactor, the gaseous CO band at 0.1 MPa is negligible. Linear CO at 2041 cm^{-1} and bridged CO at 1853 cm^{-1} were observed before the switch. No other spectral features were observed. After the switch, linear and bridged CO bands shifted to 1991 and 1813 cm^{-1}, respectively. A small dip developed on the IR spectra after 0.72 min due to incomplete compensation of the background resulting from the slight movement of the catalyst disk during the transient experiment. Due to the overlapping of the peaks and inter-

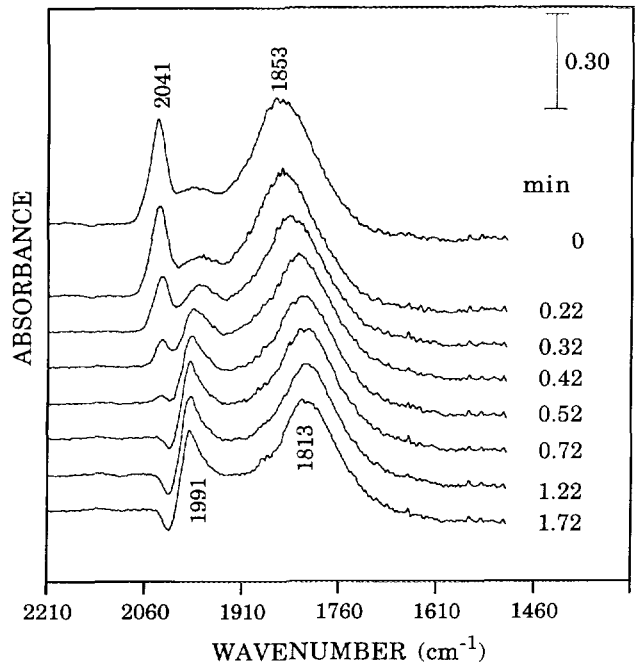

FIG. 4. Infrared spectra of steady-state isotopic transient on 3 wt% Rh/SiO_2 at 453 K and 0.1 MPa.

actions between adsorbed CO and ^{13}CO during the switch, it is difficult to deconvolute the individual peaks. It should be noted that the signal-to-noise ratio is low due to the coaddition of 5 IR scans to facilitate rapid scanning. Increasing the number of scans increases the signal-to-noise ratio but averages the transient infared spectra and loses transient information. Both linear and bridged CO appeared to switch at rates faster than the time resolution of our IR measurement. The switch from adsorbed CO to adsorbed ^{13}CO is complete in less than 0.72 min after the switch, which is consistent with the gaseous ^{13}CO response measured by the MS at 453 K. This is direct evidence that gaseous CO exchanges rapidly with the surface adsorbed CO during CO hydrogenation. The adsorbed CO exhibited the same rapid exchange behavior at 483 and 503 K. The rapid exchange between adsorbed CO and gaseous CO has also been observed for linear CO adsorbed on Ru/SiO_2 under reaction conditions of 0.1 MPa and between 443 and 493 K (46).

Pulsing CO into a Steady-State H_2 Flow

Figure 5 shows the response of effluents to a pulse of 1 cm^3 CO into a flow of 15 cm^3 H_2 and 15 cm^3 He at 503 K. The gaseous CO response exhibited a sharp pulse with a time duration of less then 0.4 min. The response of products such as H_2O and CO_2 slightly lagged behind that of CO and showed a sharp peak, similar to that of CO. The CH_4 response (shown as unconnected data points) showed an initial sharp increase in the rate of formation followed by a gradual decay. Figure 6 shows the IR spectra of adsorbed CO during the CO pulse. The spectra between 0 and 2.61 min were taken with 5 coadded scans which give a low signal-to noise ratio. As the rate of variation of IR spectra was slow after 7.2 min, 32 scans were coadded to obtain the IR spectra. A rapid adsorption of CO on the catalyst as linear CO and bridged CO exhibiting the 2042 and 1836 cm^{-1} bands, respectively, was observed during the pulsing of CO into the H_2/He stream. The intensity and wavenumbers of the linear and bridged CO bands decreased with time. The amount of CO_2 formed during the pulse at 503 K was 0.016 μmol and it was formed during the first minute of the experiment. The same studies were also carried out at 483 and 453 K. Kinetic data summarized in Table 2 will be discussed later.

The decay in the intensity of the linear and bridged CO during the CO pulse is plotted as a function of time in Fig. 7 (obtained from Fig. 6). The intensity is plotted as a fraction of the maximum intensity during the CO pulse. The linear CO intensity shows a distinct variation in slope with time. All the adsorbed CO present after the gaseous CO has been flushed from the reactor was converted to CH_4.

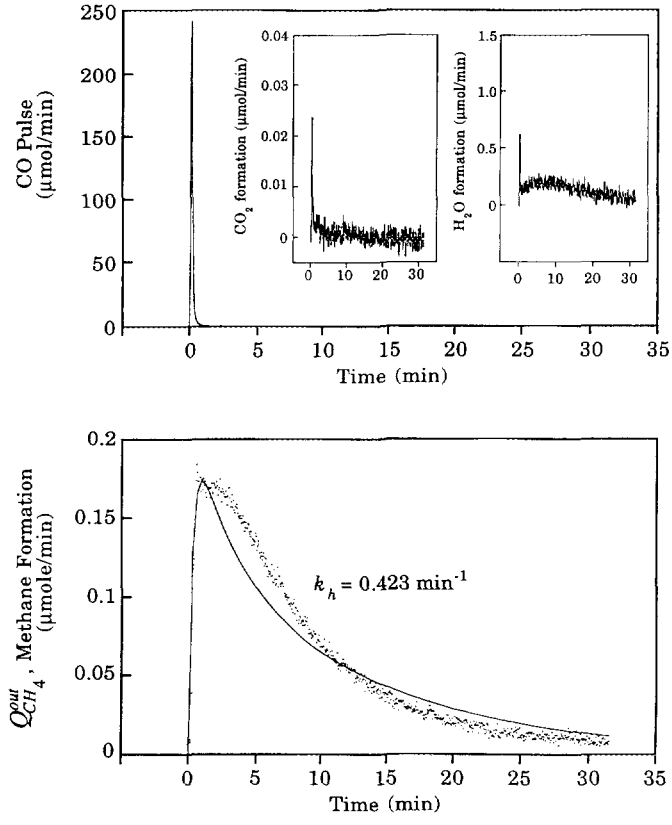

FIG. 5. Response of effluents to a pulse of CO in a steady-state H_2 flow at 503 K and 0.1 MPa.

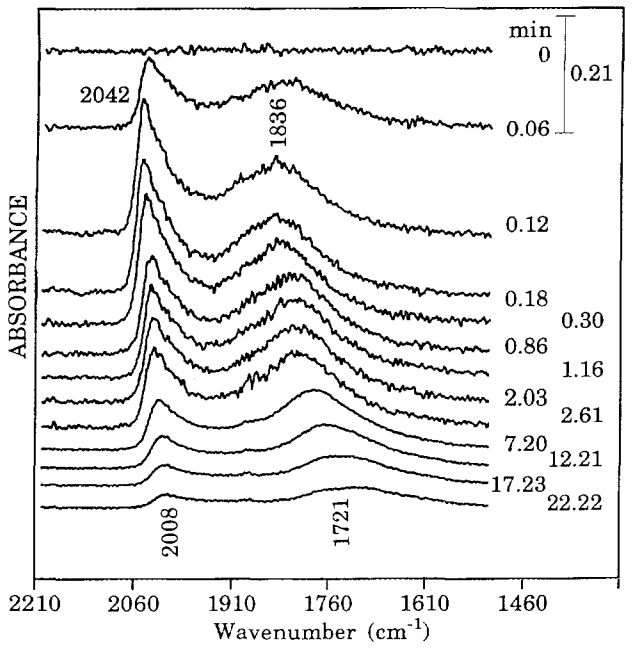

FIG. 6. Infrared spectra of a pulse of CO in a steady-state H_2 flow at 503 K and 0.1 MPa.

The response of effluents to a CO pulse into a H_2 flow at 453 and 483 K was recorded (45). The response of CH_4 closely followed that of CO at these temperatures. The amount of CO_2 formed at 483 and 453 K was 54 and 88%, respectively, of the amount of CH_4 formed, indicating that the amount of CO converted to CO_2 was substantial compared to that converted to CH_4 and could not be neglected.

ANALYSIS OF TRANSIENT DATA

Compartment Modeling of the Methanation Isotopic Transients

To analyze the transient response to the isotopic step switch, a compartment model based on the mechanism of methanation was derived. Compartment modeling has been used to describe the kinetics and transient behavior of heterogeneous catalysis as well as many other scientific investigations involving kinetic processes (17, 47).

The model representing the pathway of carbon from CO to form CH_4 is shown schematically in Fig. 8a. Each box represents a specific species in the reaction mechanism and ν_i is the reaction rate (TOF) for the elementary step i. According to the observations in the MS and corresponding IR spectra, gaseous CO is reversibly adsorbed on the surface of the catalyst. The adsorbed carbon monoxide, *CO, undergoes either desorption or dissociation and partial hydrogenation to a surface CH_x species. Because linear and bridged CO exchange rapidly with gaseous CO under steady-state conditions, only one *CO compartment is considered.

The methane response from dissociatively bonded *CO can be treated separately from the CO_2 response produced from reaction of associatively bonded *CO with *O during the steady-state transient experiment (48). Figure 5 shows that both CO_2 and H_2O exhibit rapid sharp responses, which do not permit elucidation of the role of water–gas shift reaction in methanation. Oxygen tracing studies on Ni catalyst has shown that CO_2 is produced by the direct reaction of CO with adsorbed oxygen (31). Since the mechanism of CO_2 formation remains unclear, CO_2 formation is not included in the model. Further study on oxygen tracing is required to reveal the mechanism of CO_2 formation on Rh catalyst.

Two CH_x species with distinct turnover frequencies (or reactivities) are depicted in the model. The presence of two distinct CH_x intermediates has been reported in the literature from isotopic transient and/or TPR experiments from supported Ni, Ru, and Rh catalysts (19, 37, 49, 50). The intermediates are labeled $C^{\alpha}H_x$ for the more reactive and $C^{\beta}H_x$ for the less reactive intermediate. Both CH_x intermediates are then hydrogenated to form gaseous methane. It should be noted that the transient data obtained could not fit into the model with one CH_x pathway. Soong *et al.* (19) obtained similar results for supported Ni and suggested that the data can be modeled by parallel pathways.

The model equations are derived from a molar balance of ^{13}C tracer leading to $^{13}CH_4$ in each compartment. It must be assumed that all species in each compartment react homogeneously with the same reactivity and that

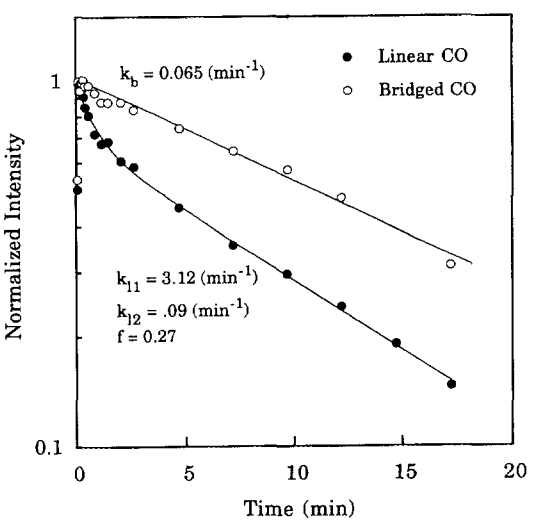

FIG. 7. Decay of linear and bridged CO normalized intensity with time to a pulse of CO in a steady-state H_2 flow at 503 K and 0.1 MPa. Normalized intensity = $(I)/(I_{max})$.

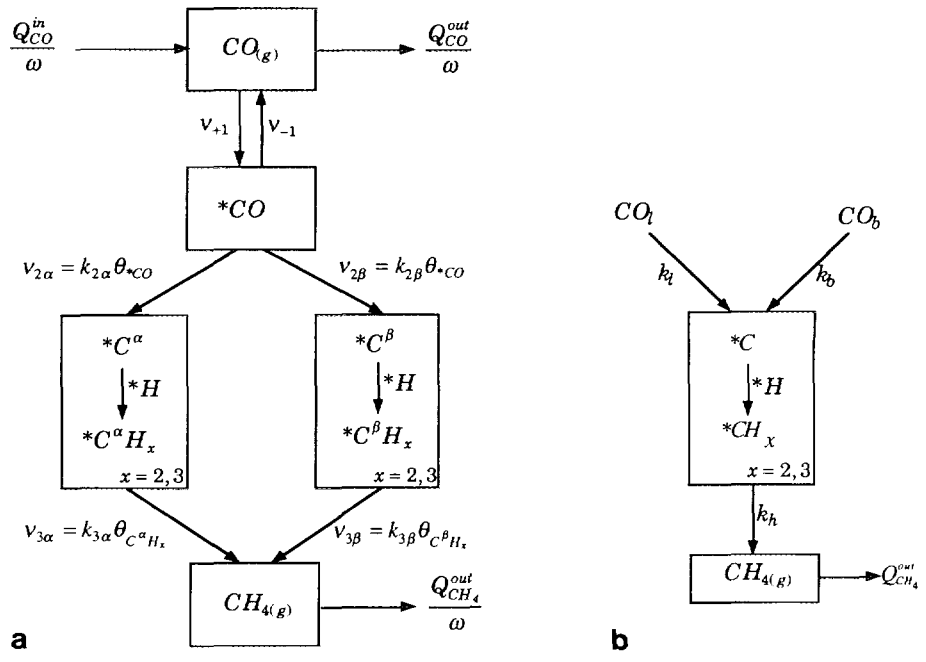

FIG. 8. (a) Schematic representation of compartment model for isotopic transient during methanation on Rh/SiO_2. (b) Schematic representation of compartment model for a pulse of CO into H_2 to form methane on Rh/SiO_2.

the species in each compartment reacts independent of the others. By defining the variable $F_i(t)$ in Eq. [1] as the fraction of the final response, the following mole balances for the tracer species in each compartment can be derived:

$$\frac{dF_{CO}}{dt} = \frac{Q_{CO}^{in}}{VC_{CO}}F_{in} + \frac{\nu_{-1}\omega}{VC_{CO}}F_{*CO} - \frac{\nu_{-1}\omega}{VC_{CO}}F_{CO} - \frac{Q_{CO}^{out}}{VC_{CO}}F_{CO} \quad [2]$$

$$\frac{dF_{*CO}}{dt} = \frac{\nu_{+1}}{\theta_{*CO}}F_{CO} - \frac{\nu_{-1}}{\theta_{*CO}}F_{*CO} - \frac{\nu_{2\alpha}}{\theta_{*CO}}F_{*CO} - \frac{\nu_{2\beta}}{\theta_{*CO}}F_{*CO} \quad [3]$$

$$\frac{dF_{*C^{\alpha}H_x}}{dt} = \frac{\nu_{2\alpha}}{\theta_{*C^{\alpha}H_x}}F_{*CO} - \frac{\nu_{3\alpha}}{\theta_{*C^{\alpha}H_x}}F_{*C^{\alpha}H_x} \quad [4]$$

$$\frac{dF_{*C^{\beta}H_x}}{dt} = \frac{\nu_{2\beta}}{\theta_{*C^{\beta}H_x}}F_{*CO} - \frac{\nu_{3\beta}}{\theta_{*C^{\beta}H_x}}F_{*C^{\beta}H_x} \quad [5]$$

$$\frac{dF_{CH_4}}{dt} = \frac{\nu_{3\alpha}\omega}{VC_{CH_4}}F_{*C^{\alpha}H_x} + \frac{\nu_{3\beta}\omega}{VC_{CH_4}}F_{*C^{\beta}H_x} - \frac{Q_{CH_4}^{out}}{VC_{CH_4}}F_{CH_4}. \quad [6]$$

In these equations, V is the gas-phase volume of the reactor, θ_i is the moles of intermediate i per mole of surface-exposed Rh metal, Q_i is the molar flow rate of the gaseous products i, and ω is the number of surface-exposed Rh atoms present in the reactor. The set of differential equations [2]–[6] and the initial conditions of $F_i = 0$ at $t = 0$ for all compartments contain all the information to describe the transient response of the isotopic tracer for any input function as long as the steady state is not disturbed.

There are nine unknown quantities in the set of differential equations, the TOF for each step and the surface coverage of each surface intermediate. The number of unknowns can be reduced when the following equations are considered under steady-state:

$$\nu_{+1} - \nu_{-1} = \frac{Q_{CH_4}^{out}}{\omega} \quad [7]$$

$$\nu_{2\alpha} = \nu_{3\alpha} \quad [8]$$

$$\nu_{2\beta} = \nu_{3\beta} \quad [9]$$

$$\nu_{3\alpha} + \nu_{3\beta} = \frac{Q_{CH_4}^{out}}{\omega}. \quad [10]$$

Equations [7]–[10] decrease the number of unknowns in the transient equations to five. The parameters were determined to be identifiable using the transfer function approach (17, 45). The parameter estimation routine in the

TABLE 1

Parameters Calculated from Steady-State Isotopic Transient Experiments

Temperature (K)	$TOF^a_{CH_4}$ (min^{-1})	τ_{*CO} (min)	$\frac{CO_2}{CH_4}$ $\left(\frac{mol}{mol}\right)$	Parameters[b]					
				ν_{+1} (min^{-1})	θ_{*CO}	$\nu_{2\alpha}$ (min^{-1})	$\theta_{*C^\alpha H_x}$	$\nu_{2\beta}$ (min^{-1})	$\theta_{*C^\beta H_x}$
453	0.0007	0.090	0.99	8.176	0.73	0.0007	0.039	—	—
483	0.0037	0.093	0.98	7.879	0.74	0.0035	0.038	0.0002	0.027
503	0.0103	0.091	0.47	8.253	0.77	0.0092	0.031	0.0011	0.061

[a] Measured from steady-state rate data.
[b] Calculated from data fit of methanation model.

TUTSIM dynamic simulation package (51) was used to solve for the unknown parameters, i.e., kinetic parameters, in Eqs. [2]–[6] for the responses in Figs. 2 and 3.

The parameters calculated from the data fit of the model for 453, 483, and 503 K and 0.1 MPa are listed in Table 1 and the solid lines in Figs. 2 and 3 are the results of the model equations. It should be noted that ν_{+1}, ν_{-1}, and θ_{*CO} are the parameters describing those CO involved in methanation. It should also be noted that $\nu_{2\alpha}$ equals $\nu_{3\alpha}$ and $\nu_{2\beta}$ equals $\nu_{3\beta}$. The rates of adsorption (ν_{+1}) and desorption (ν_{-1}) of CO on the surface are significantly greater than $\nu_{2\alpha}$ and $\nu_{2\beta}$ at all three temperatures, suggesting that adsorption and desorption of CO may approach equilibrium as compared to the rest of the elementary steps in the catalytic sequence. The high rate of adsorption and desorption of CO can also be inferred from the rapid exchange between gaseous CO and adsorbed (linear and bridge) CO. Because the rate of adsorption (ν_{+1}) and desorption (ν_{-1}) of CO remains 4 orders of magnitude greater than the net rate of CO_2 and CH_4 formation as well as $\nu_{2\alpha}$, $\nu_{2\beta}$, $\nu_{3\alpha}$, and $\nu_{3\beta}$, either inclusion or exclusion of the CO_2 formation steps into the present model will not have a significant effect on the rate of elementary steps in the model. Comparison of the rates of the hydrogenation of the CH_x intermediates, $\nu_{2\alpha}$ and $\nu_{2\beta}$, shows that most of the methane formed during steady-state conditions come from the $C^\alpha H_x$ intermediate pool. The percentage of product methane that passes through the $C^\alpha H_x$ intermediate pool decreases from 100% at 453 K to 90% at 503 K.

For comparison, the surface coverages of the intermediates calculated from the model are plotted in Fig. 9. Adsorbed CO is the most abundant surface species during steady-state CO hydrogenation. This result is consistent with literature results on supported Rh catalysts and other Group VIII metals as determined by transient and isotopic transient methods (21, 28, 37, 52). At 453 K, the surface coverage of the less reactive intermediate, $C^\beta H_x$, was found to be negligible. As temperature is increased, the coverage of $C^\beta H_x$ intermediate increases while the number of $C^\alpha H_x$ intermediate slightly decreases. Temperature-programmed reaction of Rh/Al_2O_3 revealed one type of CH_x intermediate that hydrogenates readily between 180 and 240°C and another CH_x intermediate that hydrogenates above 350°C (10). The intermediate that hydrogenates at higher temperatures is considered to be less reactive, and the amount increases with increasing reaction temperature. It is difficult to relate the $C^\alpha H_x$ and $C^\beta H_x$ observed in this study to the two intermediates in the study of Efstathiou and Bennett (10, 37) because different conditions were used. An increase in the total coverage of CH_x intermediate with an increase in temperature has been reported for Raney Ni and Ni/SiO_2 using isotopic transient experiments (18). It has been suggested that CH_x coverage is limited by the number of active sites, provided that each CH_x adsorbs on an active site (18). Increasing temperature increases the number of CH_x intermediates, suggesting an

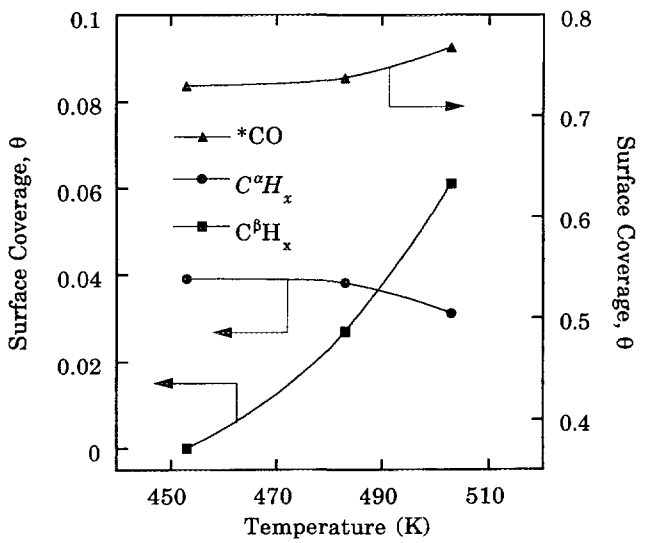

FIG. 9. Surface coverages of intermediates during methanation on 3 wt%/SiO_2 at 0.1 MPa calculated from steady-state isotopic transient results.

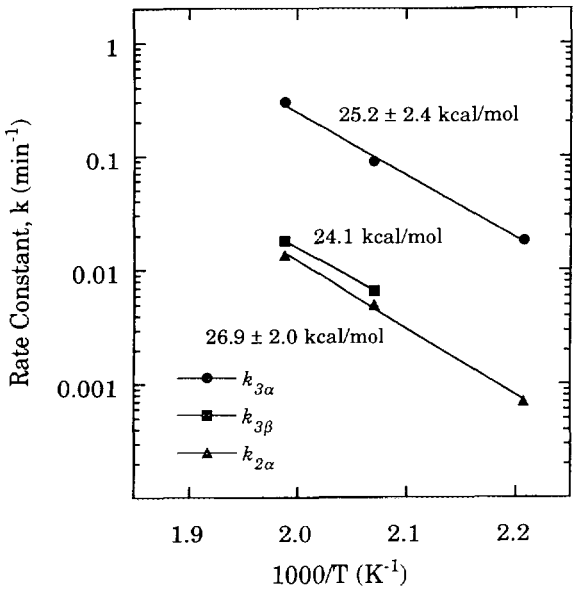

FIG. 10. Arrhenius plot of the rate constants for the elementary steps in CO hydrogenation calculated from steady-state isotopic transient data.

increase in the number of active sites. The number of active sites for adsorbed CH_x is an order of magnitude less than the sites for CO and H_2 pulse chemisorption under an inert flow at 303 K.

Assuming the rate of hydrogenation of the CH_x is first order with respect to the coverage of CH_x intermediates, rate constants for the hydrogenation step can be calculated from the equation

$$\nu_{3i} = k_i \theta_{C^iH_x}, \qquad [11]$$

where $i = \alpha$ or β. The calculated rate constants are plotted in Arrhenius form in Fig. 10. The dependence of the elementary rate constants on temperature obeys the Arrhenius law in the temperature range of the present study with the activation energies calculated to be 25.4 ± 2.4, 24.1, and 26.9 + 2.0 kcal/mol for the hydrogenation of $C^\alpha H_x$, hydrogenation of $C^\beta H_x$, and CO dissociation through the α pathway, respectively. The activation energy for the hydrogenation of $C^\beta H_x$ was estimated from two points for a rough comparison with the others. The activation energy for CO dissociation is 25% larger than that reported for Rh/SiO_2 determined by pulse surface reaction rate analysis (27). The activation energies of the hydrogenation of $C^\beta H_x$ and $C^\alpha H_x$ are similar while the reactivity of $C^\beta H_x$ is an order of magnitude less. This suggests that $C^\beta H_x$ is less accessible to adsorbed hydrogen to react toward methane. Theoretical activation energies for the hydrogenation of carbidic and partially hydrogenated surface carbon have been calculated by the bond-order-conservation Morse potential (BOC-MP) approach for single-crystal Cu, Pt, Ni, and Fe/W surfaces (53). Theoretical activation energies for this reaction on rhodium surfaces have not been reported. The theoretically derived activation energies from BOC-MP for the hydrogenation of carbidic carbon are larger than the experimental values measured in the present study on Rh by factors ranging from 1.2 for Cu to 1.8 for Fe/W.

Equation [11] assumes that the surface coverage of dissociated hydrogen, *H, is incorporated within the rate constant, that is $k_i = k_i' \theta_{*H}$, and the dependence of θ_{*H} on temperature is not significant. It is generally accepted that the adsorption of H_2 competes poorly with the adsorption of CO and the surface coverage of *H is at least an order of magnitude less than that of *CO (29, 38).

The isotopic transient experiments presented here do not provide information about the surface coverage of *H; however, information on the surface coverage of *H can be gained by a site balance of *CO and $*CH_x$. The integrated IR absorption coefficients, which relate the area under the IR band to the surface concentration of the adsorbed species, for linear and bridged CO were estimated in a previous study for the same catalyst (40, 41). Using the ratio of the linear CO to bridged CO absorption coefficients, the total surface coverage of adsorbed CO from Table 1, and the integrated areas under the linear and bridged CO IR bands, the surface coverage of each adsorbed CO can be estimated. At 503 K and 0.1 MPa the surface coverage of linear CO was found to be 0.38 while the surface coverage of bridged CO was found to be 0.39. By taking into consideration that bridged adsorbed CO takes two surface Rh sites, the total fraction of surface Rh sites taken by adsorbed CO is estimated at 1.16, which is greater than full coverage. Accounting for CH_x on the surface, the total fraction of surface Rh atoms taken up by carbon-containing intermediates is 1.25. It must be noted that the IR absorption coefficients used for this estimation contain ~20% error, which accounts for a value greater than unity. In addition, the number of exposed surface Rh atoms was measured by H_2 chemisorption at 303 K. The modification of surface structure by the reaction may contribute to uncertainty in the estimation of surface coverage. A value slightly above unity for the coverage of carbon-containing species confirms that the surface coverage of *H is small compared to that of carbon-containing intermediates and the adsorption of H_2 competes poorly with the adsorption of CO under CO hydrogenation conditions.

Surface Site Distribution Analysis

Compartment model analysis of the methanation results presented previously assumed that methane is formed along two parallel pathways, each reacting with a single

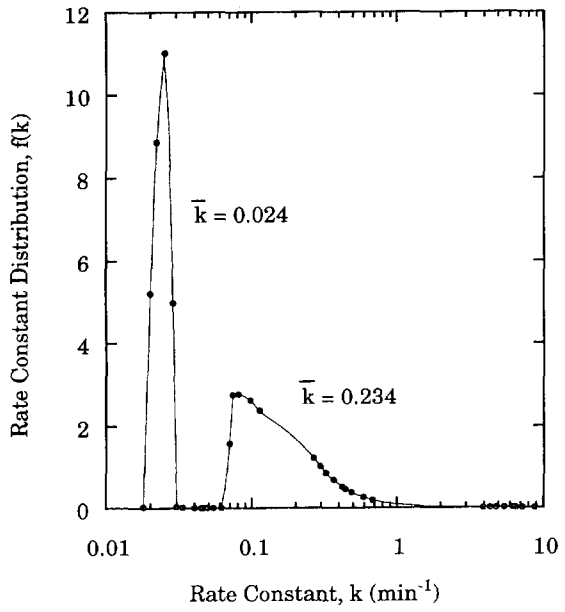

FIG. 11. Surface site distribution of methanation on 3 wt% Rh/SiO_2 at 503 K and 0.1 MPa calculated from steady-state isotopic transient data.

rate. The compartment model lumps the heterogeneity of the surface into two specific types of active sites for hydrogenation, $C^{\alpha}H_x$ and $C^{\beta}H_x$. It is reasonable to suggest that the nonuniform structure and composition of a supported metal catalyst may result in a continuous distribution of the rate constant. The distribution of rate coefficients for reactivities of the surface sites on a supported metal catalyst determines the overall activity of the metal.

Two methods have been proposed to obtain the spectrum of reactivities on a heterogeneous surface, both utilizing isotopic transient results (49, 54). The methods presented in the literature require no *a priori* knowledge of the distribution, as did the compartment model analysis, and yield discrete points along the distribution found by least-squares minimization. The disadvantage of using these approaches is that they can only be applied to a reaction that has a single rate-determining step. Intermediate pools in series with ambiguous or more than one rate-determining step are not accounted for. The method of de Pontes *et al.* (49) is applied to the results of this study. They have shown that the decay of the response can be described by

$$r^*(t) = \sum_{n=1}^{N} a_n \exp(-k_n t), \qquad [12]$$

where

$$a_n = \frac{\pi}{\omega_{max}} \theta_0^* k_n^2 f(k_n). \qquad [13]$$

The parameter ω_{max} is found from the noise level of the experimental data, θ_0^* is the surface coverage of intermediates, and $f(k)$ is a distribution of rate constants. The derivation of Eq. [12] requires that the values of k_n be spaced logarithmically between k_1 and k_N. The parameters a_n are fit to the data by least-squares approximation and the function $f(k)$ is calculated from the results.

Equations [12] and [13] were applied to the data in Fig. 3 to obtain the distribution of activity for methanation on Rh/SiO_2. The noise level of the data for the isotopic switches at 453 and 483 K was too high for consistent results. The rate constant distribution is shown in Fig. 11. The figure exhibits two distinct distributions, one with a mean value of 0.024 min^{-1} and another broad distribution with a mean value of 0.234 min^{-1}. This analysis confirms the idea that the transient data at 503 K cannot be explained by one single rate constant and verifies that two different forms of carbon with different reactivities are present on the Rh/SiO_2 surface for the methanation reaction.

Modeling of Methanation Response to Pulsing CO into H_2 Flow

Figure 8b shows the compartment model for the methane response to a CO pulse into H_2/He. The rate of disappearance of adsorbed CO during a pulse of CO into H_2 is assumed to be first order with respect to the amounts of linear and bridged CO, respectively. Lack of information and the inability to measure the rate of possible exchange between linear CO and bridge CO under reaction conditions preclude inclusion of the exchange step $CO_l \rightleftharpoons CO_b$ into the model. Although the exchange between linear and bridged CO during methanation remains to be investigated, it has been found that the exchange between adsorbed CO does not occur during ethylene hydroformylation on the same catalyst at 301 K (42). Equations are obtained for the rate of disappearance of adsorbed CO,

$$\frac{dN_{CO_l}}{dt} = -k_l N_{CO_l} \qquad [14]$$

$$\frac{dN_{CO_b}}{dt} = -k_b N_{CO_b}, \qquad [15]$$

where N_i denotes the moles of intermediate i. The rate constants of disappearance of linear and bridged CO were calculated by fitting the decay in the IR intensities shown in Fig. 7 to exponential equations, assuming the intensity is proportional to surface coverage. It must be noted, however, that the absorption coefficient is proportional to the second derivative of the dipole moment with respect to distance and may vary with surface coverage due to interactions with other adsorbates (46).

TABLE 2

Rate Parameters for Methanation during 1 cm³ CO Pulse in H_2

Temperature (K)	k_{l1} (min⁻¹)	k_{l2} (min⁻¹)	f	k_b (min⁻¹)	k_h (min⁻¹)	$Q_{CH_4}^{tot}$ (μmol)	$\frac{CO_l}{CO_b}$ $\left(\frac{mol}{mol}\right)$	$\frac{CO_2}{CH_4}$ $\left(\frac{mol}{mol}\right)$
453	2.03	0.03	0.37	0.02	—	0.12	2.54	0.88
483	6.63	0.09	0.32	0.05	—	0.40	2.10	0.54
503	3.12	0.09	0.27	0.07	0.42	1.78	2.05	0.009

The decay of the linear CO intensity shows a distinct change in slope at about 1.1 min as shown in Fig. 7, suggesting that linear CO exhibits two different reactivities. Therefore, the intensity of the linear CO band as a function of time is fitted to an exponential equation of the form

$$I = f\exp(-k_{l1}t) + (1-f)\exp(-k_{l2}t), \qquad [16]$$

where I is the fraction of maximum intensity, k_{l1} and k_{l2} are rate constants for consumption of linear CO with two different reactivities, and f is the weight fraction of linear CO that is consumed with a rate constant k_{l1}. The intensity of the bridged CO band as a function of time is fitted to an exponential equation of the form

$$I = \{\exp(-k_b t)\}, \qquad [17]$$

where I is the fraction of maximum intensity and k_b is the rate constant for consumption of bridged CO. The solid lines in Fig. 7 are least-square fits of the data to Eq. [16] and [17] at 503 K. The rate constants for the disappearance of the linear and bridged CO at 463–503 K are summarized in Table 2. The high value of k_{l1} compared to that of k_{l2} in Table 2 may be due to (i) the high rate of disappearance of the linear CO resulting from desorption and conversion to CH_4 or (ii) the variation of the absorption coefficients with the coverage of adsorbed CO. The latter case is not considered in the analysis. Figure 5 shows gaseous CO is present in the reactor for less then 0.35 min after the pulse. After 0.35 min, the CO concentration returns to the base line, indicating the absence of CO desorption.

The mole balance for carbon in the $^*C \rightarrow {}^*CH_x$ compartment leads to

$$\frac{dN_{CH_x}}{dt} = fk_{l1}N_{CO_l} + (1-f)k_{l2}N_{CO_l} + k_bN_{CO_b} - k_hN_{CH_x} \qquad [18]$$

$$Q_{CH_4}^{out} = \frac{dN_{CH_4}}{dt} = k_hN_{CH_x}, \qquad [19]$$

where N denotes the moles of respective species in the compartment. $Q_{CH_4}^{out}$ can be obtained by solving the simultaneous differential equations with the initial conditions of $N_{CH_x} = N_{CH_4} = 0$ at $t = 0$. The rate of methane formation can be expressed as

$$Q_{CH_4}^{out} = \frac{fk_{l1}k_h}{k_h - k_{l1}}N_{CO_l}^0\{\exp(-k_{l1}t) - \exp(-k_ht)\} + \frac{(1-f)k_{l2}k_h}{k_h - k_{l2}}N_{CO_l}^0\{\exp(-k_{l2}t) - \exp(-k_ht)\} + \frac{k_bk_h}{k_h - k_b}N_{CO_b}^0\{\exp(-k_bt) - \exp(-k_ht)\}, \qquad [20]$$

where $N_{CO_l}^0$ and $N_{CO_b}^0$ denote the total number of moles of linear and bridge CO when the intensity of linear and bridged CO was maximum, which is at 0.12 min. The time 0.12 min is considered a dead time for the methane response and Eq. (20) is used to fit the data taken after 0.12 min. Since the amount of CO_2 formed is less than 1% of CH_4 formed and all the CO_2 is formed within the initial 0.12 min at 503 K, it is assumed that all the adsorbed CO after 0.12 min leads to methane formation. Therefore,

$$\int_{0.12}^{\infty} N_{CH_4}\,dt = \int_{0.12}^{\infty} N_{CH_x}\,dt = N_{CO_l}^0 + N_{CO_b}^0. \qquad [21]$$

The model equations [18]–[21] can not accurately describe the dynamic behavior of the adsorbed CO and the methane formation during the presence of gaseous CO between 0 and 0.35 min. Close examination of the infrared spectra of linear and bridged CO in Fig. 6 reveals that the intensities of both species remained the same for 0.12 to 0.18 min when methane was formed, as shown in Fig. 5. During this period, the methane formed may be a result of the hydrogenation of surface carbon; in addition, the methane produced also cannot be correlated to the change in the intensity of the linear CO. The presence of gaseous CO may promote the rapid desorption and enhance the forma-

tion of methane. The amount of methane produced between 0.12 and 0.35 min is about 0.6% of the methane calculated from Eq. [21].

The ratio of the initial amounts of linear to bridged CO on the catalyst surface was calculated from the ratio of the integrated absorbances of the linear CO and bridged CO bands in Fig. 6 and the integrated absorbance coefficients for linear and bridged CO (41),

$$\frac{N^0_{CO_l}}{N^0_{CO_b}} = 2.05. \qquad [22]$$

Using Eqs. [21] and [22], the maximum amounts of linear and bridged CO were determined to be 1.2 and 0.58 μmol, respectively. The experimental data for methane formation at 503 K was fit numerically to the expression of the rate of formation of methane to obtain the value for k_h listed in Table 2. A perfect fit of the data to Eq. [20] was not obtained at 503 K since the methanation model proposed consisted of only one CH_x compartment. Increasing the number of compartments in the model would lead to an indistinguishable and unidentifiable model and the parameters would have little physical significance. Due to the large ratio of CO_2 to CH_4 formation, modeling the CH_4 response would lead to a significant error and the values of k_h at 483 and 453 K are therefore not available in Table 2.

The Equations [16] and [17] for the model presented in Fig. 8b, which considered parallel reaction of linear and bridged CO for the formation of methane, consist of three parameters. The regression of the infrared intensity data for linear and bridged CO produced an R^2 of 0.99. R^2 is determined by $R^2 = \Sigma\ (y_{\text{predicted}} - y_{\text{average}})^2/\Sigma\ (y_{\text{actual}} - y_{\text{average}})^2$, which indicates the goodness of the fit. The closer the value of R^2 to 1, the better the fit. An R^2 value of 0.97 was found for fitting the infrared intensity data to the $CO_l \rightarrow CO_b \rightarrow {}^*C \rightarrow {}^*CH_x \rightarrow CH_4$ model. Considering the $CO_l \rightleftharpoons CO_b$ will introduce additional parameters which should result in a better fitting. Due to lack of data for $CO_l \rightleftharpoons CO_b$, further data fitting is not likely to increase our understanding of the reaction.

DISCUSSION

The methanation model in Fig. 8 used to calculate the kinetic parameters is based on the mechanism of methanation on Rh-based catalysts. Two parallel CH_x pathways must be used in the model to account for the tailing of the response and to fit the data correctly. It may be argued that different reactivities of linear CO and bridged CO give rise to two different pathways leading to CH_4 during steady-state CO hydrogenation. Since linear and bridged CO exchange with gas-phase CO at rates faster than the response time of the experiments, the steady-state isotopic step transient study is not able to distinguish the reactivity of linear and bridged CO under steady state. A rapid exchange between linear and bridged CO is possible. As a result, the assumption that linear and bridged CO react as one intermediate in the model is reasonable. Pulsing CO into H_2 flow is an excellent compliment to steady-state isotopic transient study. The pulsing results listed in Table 2 demonstrate that linear CO depletes faster than bridged CO. The major mechanistic information provided from steady-state isotopic step study is the reactivity of $C^{\alpha}H_x$ and $C^{\beta}H_x$ as well as the rate-determining step.

One of the major concerns in the methanation reaction on Rh/SiO_2 is identifying the rate-determining step. The proposed mechanism for CO hydrogenation suggests that hydrocarbon and oxygenate products share a common CH_x intermediate and, in fact, complete for these intermediates (16, 55, 56). Unfortunately, the difference in activation energies for CO dissociation and hydrogenation, shown in Fig. 10, is not significant enough to determine the rate-determining step. If CO dissociation is the rate-determining step (RDS) in the methanation reaction, then control of the ratio of oxygenates to hydrocarbons may not be realized. However, if the hydrogenation of CH_x is the RDS, then the CH_x intermediate may stay on the surface long enough to allow CO insertion to occur.

By combining the response of adsorbed species measured by IR spectroscopy and the gas-phase response measured by mass spectroscopy, the rate-determining step during steady-state methanation can be inferred. In Figs. 2 and 4, it was observed that adsorbed CO and ^{13}CO exchanged rapidly on the surface of the catalyst. From the IR results, the exchange between adsorbed ^{12}CO and ^{13}CO was complete in 0.69–0.80 min, which corresponds to the response of ^{13}CO in the gas phase. Assuming the IR measured the vibrational frequencies of all adsorbed CO on the surface, the sites for adsorbed carbon monoxide were covered with only labeled ^{13}CO 0.80 min after the step switch. The gas-phase response exhibited a $^{12}CH_4$ transient that took approximately 4–10 min to complete at 453–503 K, far behind the $^{13}CO/CO$ exchange on the surface. In the absence of adsorbed ^{12}CO, the $^{12}CH_4$ produced after 0.80 min must come from slow hydrogenation of $^{12}CH_x$ intermediate. These observations indicate that the hydrogenation of the CH_x intermediate is the rate-determining step.

A major limitation of the infrared spectroscopic technique is that only the vibration of dipole moments normal to the surface is infrared active. A surface species such as

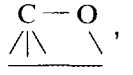

proposed as a precursor for CO dissociation (57), may not be detectable by the infrared spectroscopic technique.

Although the slow $^{13}CH_4$ response may be attributed to the slow dissociation of an adsorbed CO parallel to the surface, no spectroscopic technique has ever been able to detect such a postulated species.

The site distribution analysis also supports the notion that hydrogenation of CH_x is the rate-determining step. From Fig. 11, the distribution of rate constants reflects that of the rate-determining step since no assumptions on the mechanism is specified in the analysis. The mean values of the two distinct distributions are 0.024 min^{-1} and 0.234 min^{-1}. These values are close to 0.018 and 0.30 min^{-1} calculated for the hydrogenation of $C^{\alpha}H_x$ and $C^{\beta}H_x$ from the compartment model, suggesting that the actual rate of methanation is determined by the rate of the hydrogenation of CH_x on Rh/SiO_2 catalysts.

The data in Table 1 distinguish only the differences in reactivity and coverage between the $C^{\alpha}H_x$ and $C^{\beta}H_x$. The structure and type of active site that gives rise to these intermediates on Rh/SiO_2 cannot be deduced from the present study; however, results from the literature on other Group VIII metal catalysts can be used to elucidate the structural differences of the two CH_x species. Using Auger electron spectroscopy of a Ni(100) surface, Goodman *et al.* (35, 36) characterized the most reactive CH_x species, $C^{\alpha}H_x$, as a "carbidic" carbon, and a less reactive species, $C^{\beta}H_x$, as a "graphitic" carbon. The latter species formed above 700 K. Two separate CH_x species have also been characterized by nuclear magnetic resonance spectroscopy on Ru catalysts (58). The observed $C^{\alpha}H_x$ was deduced to be distributed on a variety of sites on or below the metal surface with $x = 0$. $C^{\beta}H_x$ was found to be partially hydrogenated ($x = 1$–3) and is made up of two separate phases with different surface mobilities. It is interesting to note that $C^{\alpha}H_x$ is distributed on a variety of sites on Ru catalyst and $C^{\alpha}H_x$ on Rh catalyst in this study exhibit a broad spectrum of activity.

From Fig. 10, the rate constant for CO dissociation is smaller than that for the hydrogenation of $C^{\alpha}H_x$ and comparable to that for the hydrogenation of $C^{\beta}H_x$. In classical kinetics, the surface coverage of an intermediate depends on site blocking by intermediates with slower reactivities. The rate of an elementary step is the product of the rate constant and the surface coverage of the intermediate involved in the reaction. A smaller rate constant means lower reactivity and possibly the rate-determining step in classical kinetics; however, for CO hydrogenation on Rh/SiO_2, this is not the case. During steady state, the rate of reaction for $C^{\alpha}H_x$ and $C^{\beta}H_x$ can be expressed as the sum of

$$\nu_{3\alpha} = k_{3\alpha}\theta_{C^{\alpha}H_x} = \nu_{2\alpha} = k_{2\alpha}\theta_{*CO} \quad [23]$$

and

$$\nu_{3\beta} = k_{3\beta}\theta_{C^{\beta}H_x} = \nu_{2\beta} = k_{2\beta}\theta_{*CO}. \quad [24]$$

The surface coverage of *CO, θ_{*CO}, includes a significant fraction of reversibly adsorbed CO that adsorbed and desorbs with a residence time of 0.09 min. This large fraction of reversibly adsorbed CO did not enter the CO dissociation pathway. In contrast, $\theta_{C^{\alpha}H_x}$ and $\theta_{C^{\beta}H_x}$ include all the CH_X that is converted to CH_4. As a result, $k_{2\alpha}$ and $k_{2\beta}$ obtained from $\nu_{2\alpha} = k_{2\alpha}\theta_{*CO}$ and $\nu_{2\beta} = k_{2\beta}\theta_{*CO}$, respectively, are not true rate constants for those adsorbed CO that are involved in methanation. The rate-determining step for methanation cannot be concluded from the relative values of $k_{2\alpha}$, $k_{2\beta}$ and $k_{3\alpha}$, $k_{3\beta}$.

In contrast to adsorbed CO in a steady-state step transient study, most of the adsorbed CO observed in the pulsing study after gaseous CO and CO_2 have left the reactor was involved in methanation. The reactivity of linear CO and bridged CO can be compared by the decay of their respective intensities with time. Modeling results at 503 K in Table 2 revealed that the rate constant for CO dissociation, k_{l2}, is smaller than that for hydrogenation, suggesting that CO dissociation is a rate-determining step under pulse conditions. It should be noted that the high value of k_{l1}, resulting from both CO desorption and dissociation in the presence of gaseous CO and possible variation of absorption coefficient, during the first minute after the pulse, does not reflect a high dissociation activity of linear CO.

A change in surface concentrations of adsorbed species appears to lead to a different elementary step being the rate-determining step. Under conditions of a pulsing study or temperature-programmed reaction conditions (24–26), the surface may contain a high concentration of *H, which in turn increases the rate of hydrogenation so that CO dissociation is the rate-determining step. The use of extinction coefficients and integrated absorbances of IR spectra show that maximum CO coverage during pulsing is 0.93. The rest of the sites are covered by *H. During steady-state conditions, the surface coverage of *H is much lower, possibly not affecting the rate of hydrogenation to a great extent. It is evident from this study that the rate-determining step is a delicate balance of intermediate concentrations, surface intrinsic properties, and reaction conditions.

At lower temperatures, the concentration of the more active site for CH_x hydrogenation is higher than that of the less active site. This fact could have implications for the design of a catalyst for higher oxygenate synthesis. Some promoters have been determined to block or electronically affect active sites on Group VIII metals (22). It may be possible to block or alter the more active methanation site to suppress methanation and increase the probability for CO insertion to occur and result in better selectivity for higher oxygenates.

CONCLUSIONS

The reactivity and the dynamics of adsorbed CO and CH_X on the Rh surface strongly depend on temperature and the partial pressure of the reactants. Steady-state transient kinetic analysis reveals the reactivity of CH_X on the surface while the pulsing CO in H_2 study reveals the reactivity of linear and bridged CO for methanation. By comparison of the IR spectra and the gas-phase response of a $CO/^{13}CO$ switch, it was found that gaseous CO exchanges rapidly with surface adsorbed CO, both linear and bridged, and that the hydrogenation of CH_x is the rate-determining step during steady-state CO hydrogenation. Both compartment modeling and surface site distribution analysis support this conclusion. These two different methods of analysis also show that CH_x intermediate hydrogenates to CH_4 with two distinct rate constants. Pulsing CO in H_2 flow shows that the linear CO depletes faster than bridged CO and CO dissociation is the rate-determining step for methanation due to the high coverage of adsorbed hydrogen. Combined *in situ* infrared study with steady-state isotopic transient analysis and pulsing CO into H_2 flow allow us to draw a definite conclusion that different operating conditions lead to a different rate-determining step. Mechanistic and kinetic studies of catalytic reactions have to be performed under practical reactor conditions.

ACKNOWLEDGMENT

The authors gratefully acknowledge the support of this research by the U.S. Department of Energy under Grant DG-FG-87PC79923.

REFERENCES

1. Bache, R. A., Gray, W. M., and Smith, D. J., *IEEE Proc.* **128**(Part D), 56 (1981).
2. Berck, P. D., Bloomer, J. R., Howe, R. B., and Berlin, N. I., *Am. J. Med.* **49,** 296 (1970).
3. Boxenbaum, H. G., and Riegelman, S., *J. Pharmacokinet. Biopharm.* **4,** 287 (1976).
4. Steinfeld, J. L., Fransisco, J. S., and Hase, W. L. "Chemical Kinetics and Dynamics." Prentice-Hall, Englewood Cliffs, NJ, 1989.
5. Levenspiel, O., and Bischoff, K. B., *in* "Advances in Chemical Engineering." (T. B. Drew, J. W. Hoopes Jr., and T. Vermeulen, Eds.), Vol. 4, p. 95. Academic Press, New York, 1963.
6. Aris, R., "Elementary Chemical Reactor Analysis." Prentice Hall, Englewood Cliffs, NJ, 1963.
7. Wen, C. Y., and Fan, L. T., "Models for Flow Systems and Chemical Reactors." Dekker, New York, 1975.
8. Luyben, W. L., "Process Modeling, Simulation, and Control for Chemical Engineers," 2nd ed. McGraw-Hill, New York, 1990.
9. Tamaru, K., *in* "Catalysis: Science and Technology," (J. R. Anderson and M. Boudart, Eds.), Vol. 9, p. 87, Springer Verlag, Berlin/Heidelberg/New York, 1991.
10. Efstathiou, A. M., and Bennett, C. O., *J. Catal.* **120,** 118 (1989).
11. Mori, Y., Mori, T., Takahashi, N., Hattori, T., and Murakami, Y., *J. Phys. Chem.* **94,** 4575 (1990).
12. Kaul, D. J., and Wolf, E. E., *J. Catal.* **89,** 348 (1984).
13. Li, Y. E., Willcox, D., and Gonzalez, R. D., *AIChE J.* **35,** 423 (1989).
14. Vannice, M. A., *Catal. Rev. Sci. Eng.* **14**(2), 153 (1976).
15. Ponec, V., *Catal. Rev. Sci. Eng.* **18**(1), 151 (1978).
16. Bell, A. T., *Catal. Rev. Sci. Eng.* **23**(1&2), 203 (1981).
17. Happel, J., "Isotopic Assessment of Heterogeneous Catalysis." Academic Press, New York/London, 1986.
18. Yang, C. H., Soong, Y., and Biloen, P., *in* "Proceedings, 8th International Congress on Catalysis, Berlin, 1984," Vol. 2, p. 3. Dechema, Frankfurt-am-Main, 1984.
19. Soong, Y., Krishna, K., and Biloen, P., *J. Catal.* **97,** 330 (1986).
20. Stockwell, D. M., Chung, J. S., and Bennett, C. O., *J. Catal.* **112,** 135 (1988).
21. Siddall, J. H., Miller, M. L., and Delgass, W. N., *Chem. Eng. Comm.* **83,** 261 (1989).
22. Hindermann, J. P., Hutchings, G. J., and Kiennemann, A., *Catal. Rev. Sci. Eng.* **53**(1), 1 (1993).
23. Stuchly, V., and Klusacek, K., *J. Catal.* **139,** 62 (1993).
24. McCarty, J. G., and Wise, H., *J. Catal.* **57,** 406 (1979).
25. Ho, S. V., and Harriott, P., *J. Catal.* **64,** 272 (1980).
26. Ozdogan, S. Z., Gochis, P. D., and Falconer, J. L., *J. Catal.* **83,** 257 (1983).
27. Koerts, T., Welters, J. J., and van Santen, R. A., *J. Catal.* **134,** 1 (1992).
28. Koerts, T., and van Santen, R. A., *J. Catal.* **134,** 13 (1992).
29. Araki, M., and Ponec, V., *J. Catal.* **44,** 439 (1976).
30. Biloen, P., Helle, J. N., and Sachtler, W. M. H., *J. Catal.* **58,** 257 (1979).
31. Happel, J., Suzuki, I., Kokayeff, P., and Fthenakis, V., *J. Catal.* **65,** 59 (1980).
32. Cant, N. W., and Bell, A. T., *J. Catal.* **73,** 257 (1982).
33. Happel, J., Cheh, H. Y., Otarod, M., Ozawa, S., Severdia, A. J., Yoshida, T., and Fthenakis, V., *J. Catal.* **75,** 314 (1982).
34. Biloen, P., Helle, J. N., van den Berg, A., and Sachtler, W. M. H., *J. Catal.* **81,** 450 (1983).
35. Goodman, D. W., Kelley, R. D., Madey, T. E., and Yates, J. T., Jr., *J. Catal.* **63,** 226 (1980).
36. Goodman, D. W., Kelley, R. D., Madey, T. E., and White, J. M., *J. Catal.* **64,** 479 (1980).
37. Efstathiou, A. M., and Bennett, C. O., *J. Catal.* **120,** 137 (1989).
38. Underwood, R. P., and Bennett, C. O., *J. Catal.* **86,** 245 (1984).
39. Anderson, J. R., and Pratt, K. C., "Introduction to Characterization and Testing of Catalysts." Academic Press, New York/London, 1985.
40. Srinivas, G., Chuang, S. S. C., and Balakos, M. W., *AIChE J.* **39,** 530 (1993).
41. Srinivas, G., and Chuang, S. S. C., *J. Catal.* **144.** 131 (1993).
42. Chuang, S. S. C., and Pien, S. I., *J. Catal.* **135,** 618 (1992).
43. Ellgen, P. C., Bartley, W. J., Bhasin, M. M., and Wilson, T. P., *Adv. Chem. Ser.* **178,** 147 (1979).
44. Underwood, R. P., and Bell, A. T., *J. Catal.* **111,** 325 (1988).
45. Balakos, M. W., Ph.D. dissertation, The University of Akron, Ohio, 1994.
46. Winslow, P., and Bell, A. T., *J. Catal.* **86,** 158 (1984).
47. Godfrey, K., "Compartment Models and Their Applications." Academic Press, New York/London, 1983.
48. Otarard, M., Ozawa, S., Yin, F., Chew, M., Chen, H., and Happel, J., *J. Catal.* **84,** 156 (1983).
49. de Pontes, M., Yokomizo, G. H., and Bell, A. T., *J. Catal.* **104,** 147 (1987).
50. Glugla, P. G., Bailey, K. M., and Falconer, J. L., *J. Phys. Chem.* **92,** 4474 (1988).
51. Reynolds, W. E., and Wolf, J., "TUTSIM Block Diagram Simulation Language," TUTSIM Products, Palo Alto, CA, 1991.
52. Jackson, S. D., Brandreth, B. J., and Winstanley, D., *J. Catal.* **106,** 646 (1987).
53. Shustorovich, E., and Bell, A. T., *Surf. Sci.* **248,** 359 (1991).

54. Hoost, T. E., and Goodwin, J. G., Jr., *J. Catal.* **134,** 678 (1992).
55. Chuang, S. C., Tian, Y. H., Goodwin, J. G., Jr., and Wender, I., *J. Catal.* **96,** 449 (1985).
56. Sachtler, W. M. H., and Ichikawa, M., *J. Phys. Chem.* **90,** 4752 (1986).
57. Hindermann, J. P., Kiennemann, A., Cakor-Alami, A., and Kieffer, R., *in* "Proceedings, 8th International Congress on Catalysis, Berlin, 1984," Vol. 2, p. 163. Dechema, Frankfurt-am-Main, 1984.
58. Duncan, T. M., Winslow, P., and Bell, A. T., *J. Catal.* **93,** 1 (1985).